Analysis of Dynamic Impatt Oscillations caused by Radiation Induced Deep Centers with Local and Homogenous Vertical Distribution

Ralf Siemieniec[1], Josef Lutz[2], Reinhard Herzer[3]

[1]Institute of Solid-State Electronics, Technische Universitaet Ilmenau, PO Box 100565, D - 98684 Ilmenau, Germany, Phone: +49 3677 693225, Fax: +49 3677 693777, e-mail: ralf.siemieniec@tu-ilmenau.de

[2]Faculty of Electrical Engineering and Information Technology, Technical University of Chemnitz, D-09107 Chemnitz, e-mail: josef.lutz@infotech.tu-chemnitz.de

[3]SEMIKRON Elektronik GmbH, Sigmundstraße 200, D-90431 Nuernberg, Germany, e-mail:reinhard.herzer@semikron.com

Abstract

The occurrence of high-frequency impatt oscillations is related to the presence of charged deep donor-states as generated by irradiation processes for carrier-lifetime control. This effect is well-known in electron-radiated devices. Device simulation predicts a similar effect in locally lifetime-controlled helium-radiated devices. The experiment gives an approval of the simulation results, but shows some unexpected effects as well. An analytical estimation sufficiently predicts the temperature dependence of the threshold voltage for the onset of the oscillations.

1 Introduction

Transit-time oscillations in modern bipolar power devices are caused by different mechanisms and could result in an annoyance of drive control units [1] as well as in an dramatic increase of electromagnetic radiation [2]. In difference to oscillations due to a current snap-off during turning off a power device (LC oscillations) or due to harmonics, transit-time oscillations are high-frequency oscillations in the range of 200MHz ... 1GHz.

Impatt (impact ionisation transit time) oscillations are well-known from Impatt- and other comparable transit-time diodes [3]. Here, a high-frequency signal is generated at a voltage above the stationary avalanche breakdown voltage. Another mechanism is the one used in Baritt (barrier injection transit time) diodes [4], where holes are injected into the space charge region from the p^+-region of the diode. Related to that is the relatively newly discovered Pett (plasma extraction transit time) oscillation [5]. In contrast to the Baritt effect, the carrier injection into the space charge region is caused by stored excess carriers in the remaining plasma of the device during the turn-off process. Pett oscillations were first observed in modules with paralleled IGBT chips [5], but meanwhile there were also found at paralleled freewheeling diodes and even in single chips [6].

In difference, this paper is about dynamic impatt oscillations. These are high-frequency oscillations which occur in carrier-lifetime controlled silicon power devices in the low working temperature range (app. T<280K) at voltages well below the static breakdown voltage [1]. They are caused by temporarily positive charged deep donors H(195K) – related to the carbon-vacancy complex COVV – which are induced by irradiation and annealing.

Although this type of transit-time oscillation is expected to occur at low temperatures, outside the usual working temperature range of power devices, such failures may happen in systems working under rough environmental conditions. This are, as example, a building crane or a electric locomotive at low temperatures in winter time. If dynamic impatt oscillations occur, the electromagnetic radiation generated by the oscillations interferes with the drive-control and other electronic units, leading to a stop of the power converter. The avoidance of these high-frequency oscillations therefore is necessary because of their strong adverse influence on the drive control units and because of EMC issues [2].

2 Experimental Setup

Measurements are done using a conventional double-pulse method. All devices have a doping profile as shown in Fig. 1. After irradiation, all samples are annealed at T>600K for 1h. Fig. 2 gives an example of a measured impatt oscillation of an electron-radiated diode (E=4.5MeV, d=1E15cm^{-2}).

3 Simulation Model

Irradiation processes generate a number of centers with different energy levels in the band gap of Silicon. Each generated level could act as a recombination center where the total recombination rate depends on the emission and capture processes of each single level [9]. For all simulations, the 2D device simulator TeSCA has been used [7]. This simulation system solves the three fundamental semiconductor equations, which had been extended to consider deep traps as well as their time-dependent charging processes as described elsewhere [8-10]. Based on this model it is possible to predict the

behaviour of radiated devices with qualitatively and quantitatively good results which is the precondition for the work presented in this paper.

4 Properties of Radiation Induced Centers

The knowledge of recombination center properties is essential for simulation purposes as well as for the understanding of the device behaviour. In previous work, much efforts were spend for the determination of the recombination center parameters [9,10]. Table 1 shows the properties of the relevant recombination centers as used in the simulations. The fundamental properties of the radiation-induced centers were determined using DLTS (deep level transient spectroscopy) measurements [11]. Since power devices are usually operated at high injection levels, it is necessary to know the parameters of the dominant recombination centers for a wide temperature range. In the devices investigated in this work, the center E(90K) controls the carrier lifetime under high-injection condition which allows the use of high-level carrier lifetime measurements. Using the well known OCVD (open circuit voltage decay) measurement technique [12] in combination with optical excitation of free carrier pairs to generate a large density of excess carriers, it was possible to determine the capture rates of E(90K) over a wide temperature range [9,13]. In case of the other recombination centers E(230K) and H(195K), the temperature dependencies of the capture rates are extrapolated from the DLTS data. Since these centers are characterised at higher temperatures, compared to E(90K), the deviations caused by the extrapolation are assumed to be smaller.

5 Investigation of electron-radiated devices

Fig. 3 shows a simulation of an impatt oscillation, using a simple series circuit of a time-variable resistor, a small inductance and an electron-radiated diode structure according to Fig. 1 (E=4.5MeV, d=1E15cm^{-2}). During the turn-off, the generated donor-states are positively charged and increase the background doping, which usually sustains the blocking voltage. Avalanche breakdown occurs at the pn-junction region due to the high electric field, which is shown in Fig. 4 for several points in time, and generates electrons. These electrons counterbalance the positive donors and hence stop the avalanche generation of carriers. Therefore, the avalanche generation rate changes with time. Due to the electric field, the electrons are transported to the nn$^+$-junction and again, avalanche generation starts at the pn-junction.

Fig. 5 shows the electron densities along the vertical axis for different points in time. The frequency of the oscillation is related to the transit-time which is needed by the electron flow through the low-doped region of the device, depending on the carrier saturation velocity v_d and the width of the low-doped region w_B:

$$f \approx \frac{v_d}{w_B} \tag{1}$$

The measured oscillation frequency for the electron-radiated device (see Fig. 2) is in the range of 850...950MHz in agreement with [1]. The determination of the frequency is difficult due to interfering noise and resolution capability.

The impatt oscillation stops as soon as the positive donors are discharged, according to the time constant which depends on the center concentration and the capture rates. The device is now able to withstand the reverse voltage [1]. Fig. 7 shows the reduction of density of the charged donor-states with time.

The onset of this effect depends mainly on the concentration of the deep donors and of the temperature. Fig. 7 shows the comparison of measured and simulated values of the onset voltage of impatt oscillations on electron-radiated recovery diodes. The simulated and measured values show a sufficient accordance.

6 Investigation of helium-radiated devices

For local recombination center profiles (as generated by use of helium ions) in the low-doped region of the device, device simulation predicts the occurrence of impatt oscillations. Fig. 8 gives the center profiles as used in the preliminary simulations. Fig. 9 shows, as an example, one result of the device simulations for a diode with a deep local recombination center profile. Obviously, dynamic impatt oscillations may occur even in devices with a local recombination center profile.

For an experimental verification of the simulation results, devices were manufactured. Helium irradiation with an energy of 11MeV was applied from the top side to samples with an active area of $0.1cm^2$. Two different radiation doses of $1.4 \cdot 10^{12}$ cm^{-2} and $2.1 \cdot 10^{12}$ cm^{-2} are used (further referring to samples He14 and He21, respectively).

Fig. 10 shows a measurement of an impatt oscillation at the device He21. In difference to electron-radiated devices, additional two current peaks are to be seen before the oscillation starts. There is no sharp threshold voltage of the oscillation at the samples He21. The voltage amplitude of the oscillation is much lower for helium-radiated devices compared to electron-radiated devices. The oscillation frequency, app. 1.4...1.6GHz in the measurement of He21, is higher compared to the oscillation frequency of electron-radiated samples.

7 Temperature Dependence of Threshold Voltage

7.1 Experimental Results

A qualitative explanation for the different behaviour of the helium-radiated devices is given by the simulation results of structures with a recombination center profile as shown in fig. 8. Fig. 11 shows the electric field at different points in time which is now trapezoidal as it were in presence of an additional n-doped buffer layer. This is caused by the ionised donor-states, shown in Fig. 12, which obviously act as a kind of temporarily buffer layer. Thus, the width of the low-doped region is reduced and the oscillation frequency rises.

There is no definite threshold voltage in case of the helium-radiated samples. The oscillation starts almost inappreciable and is therefore difficult to measure due to the interfered noise. Consequently, the reverse voltage is measured at a condition, where the avalanche-related current peak reaches a previously assigned value. Fig. 13 shows the temperature dependent voltage for an avalanche current density of 30A/cm^2. Now, in case of helium-radiated samples, in the investigated temperature range the temperature coefficient of the avalanche threshold voltage is found to have a mean value of 1.8V/K. In contrast, in electron-radiated devices this value was measured to be 2.9V/K.

7.2 Analytical Estimation

The changed shape of the electric field, trapezoidal instead of triangular, results in a weaker temperature dependency of the avalanche generation. An analytical estimation is based on an abrupt junction and the impact ionisation coefficients in [14] with the temperature dependency given in [15]:

$$\alpha_{eff}(E) = c \cdot |E|^{b} \tag{2}$$

$$c = 2 \cdot 10^{-28} \exp\left(-16.22 \frac{T}{300K} \right) cm^6 V^{-7} \tag{3}$$

$$b = 5.8 + 1.2 \frac{T}{300K} \tag{4}$$

In case of a triangular-shaped electric field, the field strength results from:

$$E(w) = \frac{qN_D}{\varepsilon_0 \varepsilon_r} \left(w - w_B \right) \tag{5}$$

Impact ionisation occurs, if the integration of eq. (2) along the base width of the device results to one. Eq. (2) to (5) lead to the relation between the avalanche breakdown voltage V_{DI} in dependence of the effective doping:

$$V_{DI} = \frac{1}{2} \left(\frac{b+1}{c} \right)^{\frac{2}{b+1}} \left[\frac{q\left[N_D + N_{TD}{}^{+}(T,t) \right]}{\varepsilon_0 \varepsilon_r} \right]^{\frac{1-b}{1+b}} \tag{6}$$

The density of the charged donor-states N_{TD}^{+} depends on temperature and time [1]. During the conducting state, the deep donors are occupied with holes and the positively charged donor concentration is determined from the stationary rate equation to:

$$N_{TD,0}{}^{+}(T, t=0) = \frac{N_{TD}}{1 + \frac{c_n(T)}{c_p(T)}} \tag{7}$$

According to the values given in Table 1, the density of charged donor-states results in a weak temperature dependence in the temperature range as used for the characterisation of dynamic impact oscillations. Consequently, the temperature dependence of the threshold voltage V_{DI} is mainly due to the temperature dependency of the impact ionisation and of the thermal emission of holes after the reverse recovery current peak. The positively charged deep donor states discharge with a time constant proportional to the reciprocal emission rate of holes e_h:

$$N_{TD}{}^{+}(T,t) = N_{TD} \exp\left[-e_h \left(t_d - t_{RRM} \right) \right] \tag{8}$$

Here, t_d describes the delay time until the reverse voltage reaches it's final value. The value of t_{RRM} is the point in time, where the reverse recovery current maximum is found. For the determination of the onset voltage of the dynamic impatt oscillation, measurements with high di/dt were used. In these measurements, the switching behaviour of the IGBT is characterised by a mean value of t_d-t_{RRM} of 200ns.

The temperature dependence of the threshold voltage for the onset of impact ionisation of the electron-radiated device could be estimated using the recombination center properties of H(195K) as shown in Table 1 and eq. (6) to eq. (8), since the electric field is triangular (see fig. 4). Under this conditions, a mean value of 2.3V/K is found compared to the measured value of 2.9V/K.

In case of an trapezoidal-shaped electric field, the field-strength along the vertical direction of the device results from:

$$E(w) = -E_{nn+} + \frac{qN_D}{\varepsilon_0 \varepsilon_r}\left(w - w_B\right) \tag{9}$$

According to fig. 1, E_{nn}^{+} is the field strength found at the nn^{+}-junction. The integration of eq. (2) after inserting eq. (9) and solving for the case of impact ionisation leads to:

$$\left(E_{nn+} + \frac{qN_D}{\varepsilon_0 \varepsilon_r} w_B\right)^{(b+1)} - {E_{nn+}}^{(b+1)} = (b+1)\frac{qN_D}{\varepsilon_0 \varepsilon_r c} \tag{10}$$

A analytical solution of eq. (10) is possible, if the field strength at the nn^{+}-junction E_{nn+} is reasonable small compared to the field strength E_{pn} at the pn-junction side [16], or:

$${E_{nn+}}^{(b+1)} << {E_{pn}}^{(b+1)} \tag{11}$$

The field strength E_{pn} obviously results from:

$$E_{pn} = E_{nn+} + \frac{qN_D}{\varepsilon_0 \varepsilon_r} w_B \tag{12}$$

while the breakdown voltage in case of a trapezoidal-shaped field is:

$$V_{BD} = \frac{E_{pn} + E_{nn+}}{2} w_B \tag{13}$$

Finally, using eq. (9) to eq. (13), the avalanche breakdown voltage dependency in this case is given by:

$$V_{DI} = \left[\frac{(b+1)q\left[N_D + {N_{TD}}^{+}(T,t)\right]}{\varepsilon_0 \varepsilon_r c} \right]^{\left(\frac{1}{b+1}\right)} w_B - \frac{1}{2} \frac{q\left[N_D + {N_{TD}}^{+}(T,t)\right]}{\varepsilon_0 \varepsilon_r} {w_B}^2 \tag{14}$$

In difference to the electron-radiated devices, the donor concentration and it's distribution profile along the vertical axis is not known. DLTS measurements are not suitable for recombination center concentrations larger than the doping density, and even recently proposed current transient spectroscopy (CTS) measurements [17] fails due to compensating effects. Therefore, it is necessary to use the estimated center distribution profile as provided for the simulations. Under this precondition, the base width w_B was extracted from the simulation results as well. Finally, the suchlike estimated temperature dependence of the threshold voltage for the onset of impact ionisation in case of a trapezoidal-shaped electric field is found to have a mean value of 1.2V/K. The value found in the measurements was 1.8V/K.

Taking into account the simplifications incorporated into the analytical expressions, especially in case of the trapezoidal-shaped electric field (unknown recombination center distribution), the temperature coefficients according to the analytical estimations are in sufficient accordance with the measured values. The results of the analytical derivation give evidence to the assumption, that a temporarily buffer-layer is formed by charged deep traps.

8 Conclusion

In this work, the occurrence of dynamic impatt oscillations in homogenous and locally carrier-lifetime controlled devices is analysed by means of device simulation and compared with experimental results. Such oscillations, effected by temporarily charged deep levels, are therefore found in electron-radiated devices as well as in devices applied to high-energy helium irradiation. The specific behaviour of the helium-radiated devices is explained by the formation of a temporarily n-buffer due to the temporarily positively charged donor-states of generated centers, leading to a different shape (trapezoidal instead of triangular) of the electric field. An analytical estimation of the temperature coefficient for the onset voltage of the dynamic impatt oscillation, based on the different field shapes, results in a sufficient accordance to the measured values.

To avoid these oscillations, it is necessary to restrict the number of generated donor-states in accordance to the desired voltage range of the device. Therefore, irradiation parameters as well as annealing temperature and time have to be chosen carefully.

References

[1] Lutz, J., Südkamp, W. and Gerlach, W.: Impatt Oscillations in Fast Recovery Diodes due to Temporarily Charged Radiation-Induced Deep Levels, *Solid-State Electronics*, 42 (6), 1998, 931-938

[2] Siemieniec, R., Lutz, J., Netzel, M., Mourick, P.: Transit Time Oscillations as a Source of EMC Problems in Bipolar Power Devices, *Proc. EPE* (Toulouse 2003)

[3] Sze, S.M.: *Physics of Semiconductor Devices*, 2nd Edition, John Wiley & Sons, New York, 1981

[4] van de Roer, T.G.: *D.C. and small-signal A.C. properties of silicon BARITT diodes*, Ph.D. Thesis, University of Eindhoven, 1977

[5] Gutsmann, B., Mourick, P. and Silber, D.: Plasma Extraction Transit Time Oscillations in Bipolar Power Devices, *Solid-State Electronics*, 46 (5), 2002, 133-138

[6] Mourick, P., Gutsmann, B, and Silber, D.: Ultra High Frequency Oscillations in the Reverse Recovery Current of Fast Diodes, *Proc. ISPSD (Santa Fee 2002)*, 205-208

[7] Gajewski, H., Heinemann, B. and Langmach, H.: *TeSCA-Handbuch*, Weierstrass-Institute for Applied Analysis and Stochastics, Berlin, 1991-2003

[8] Siemieniec, R. and Lutz, J.: Possibilities and limits of axial lifetime control by radiation induced centers in fast recovery diodes, *Microelectronics Journal*, 35, 2004, 259-267

[9] Siemieniec, R., Südkamp, W. and Lutz, J.: Determination of Parameters of Radiation Induced Traps in Silicon, *Solid-State Electronics*, 46(6), 2002, 891-901

[10] Siemieniec, R., Südkamp, W. and Lutz, J.: Applying Device Simulation for Lifetime-Controlled Devices, *Proc. ICCDCS 2002 (Aruba 2002)*

[11] Lang, D.V.: Deep-Level Transient Spectroscopy: A New Method to Characterize Traps in Semiconductors, *Journal of Applied Physics*, 45(7), 1974, 3023-3032

[12] Lederhandler, S.R. and Giacoletto, L.J.: Measurement of Minority Carrier Lifetime and Surface Effects in Junction Devices, *Proc. IRE (1955*), 477-483

[13] Siemieniec, R.: *Simulation von Leistungsbauelementen mit durch Bestrahlungs-verfahren eingestellter Trägerlebensdauer*, Ph.D. Thesis TU Ilmenau, BoD GmbH Norderstedt, 2003

[14] Fulop, W.: Calculations of Avalanche Breakdown Voltages of Silicon pn-Junctions, *Solid-State Electronics*, 10, 1967, 39-42

[15] Singh, R. and Baliga, B.J.: Analysis and optimization of power MOSFETs for cryogenic operation, *Solid-State Electronics*, 36(8), 1993, 1203-1211

[16] Lutz, J.: *Freilaufdioden für schnell schaltende Leistungsbauelemente*, Ph.D. Thesis TU Ilmenau, Verlag ISLE, 2000

[17] Hazdra, P., Brand, K. and Vobecký, J.: Defect distribution in MeV proton irradiated silicon measured by high-voltage current transient spectroscopy, *Nuclear Instruments and Methods in Physics Research B*, 192, 2002, 291-300

Tables

Table 1: Recombination center properties

Trap	Energy level	Capture coefficients	
		c_n [cm^3/s]	c_p [cm^3/s]
E(90K)	E_C-E_T=0.167eV	$1.15 \cdot 10^{-7} \exp\left(-\frac{T}{355.4K}\right)$	$6.39 \cdot 10^{-7} \sqrt{\frac{T}{300K}} \exp\left(\frac{6.15 \cdot 10^{-3}\ eV\ K}{k_B T}\right)$
E(230K)	E_C-E_T=0.447eV	$3.41 \cdot 10^{-8} \sqrt{\frac{T}{300K}} \exp\left(\frac{22.13 \cdot 10^{-3} eV\ K}{k_B T}\right)$	$2.79 \cdot 10^{-8} \sqrt{\frac{T}{300K}} \exp\left(-\frac{22.13 \cdot 10^{-3}\ eV\ K}{k_B T}\right)$
H(195K)	E_T-E_V=0.351eV	$9.85 \cdot 10^{-9} \sqrt{\frac{T}{300K}} \exp\left(-\frac{85 \cdot 10^{-3}\ eV\ K}{k_B T}\right)$	$4.3 \cdot 10^{-9} \sqrt{\frac{T}{300K}}$

Figures

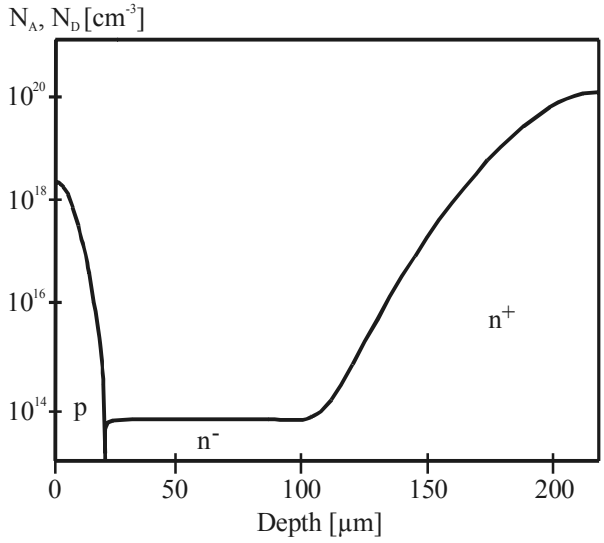

Fig. 1: Basic structure of 1200V, 150A/cm^2 diode

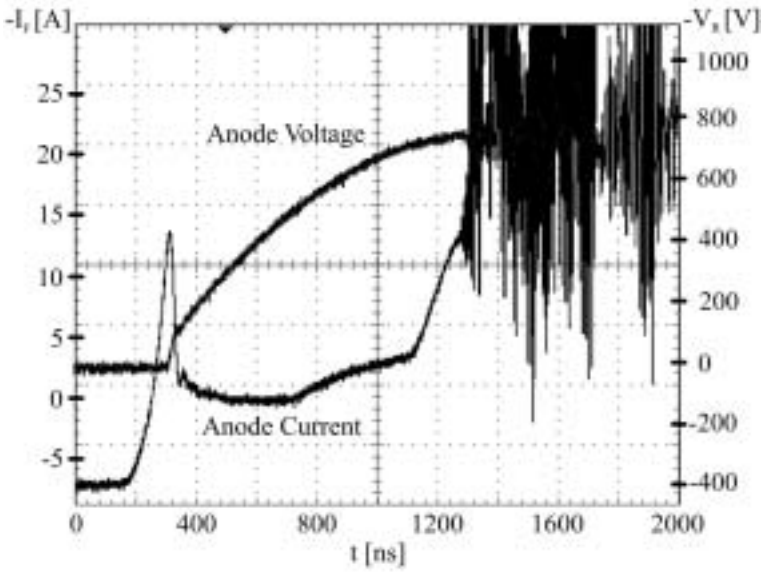

Fig. 2: Oscillogram of an impatt oscillation, T=275K, V_R=790V, J_F=15A/cm^2 (5A/div, 200V/div, 200ns)

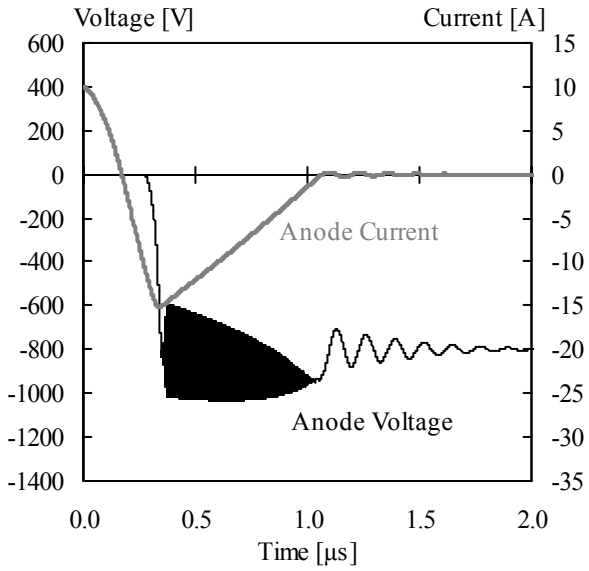

Fig. 3: Simulation of temporary impatt oscillation, T=300K, V_R=800V, J_F=15A/cm^2

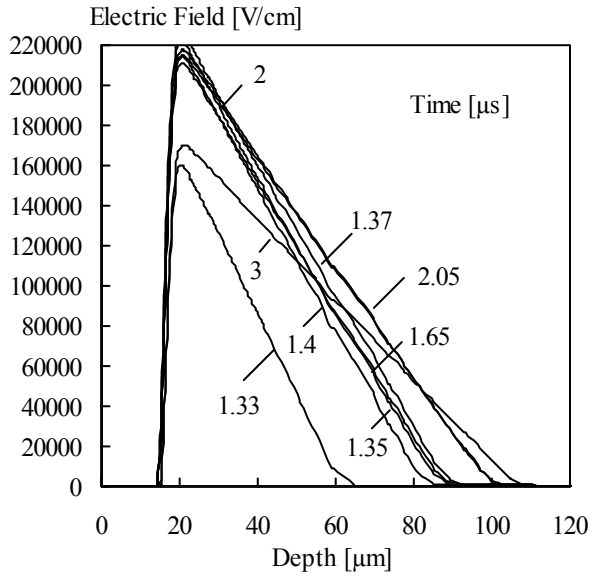

Fig. 4: Electric Field along vertical axis vs. time, T=300K, V_R=800V, J_F=15A/cm^2

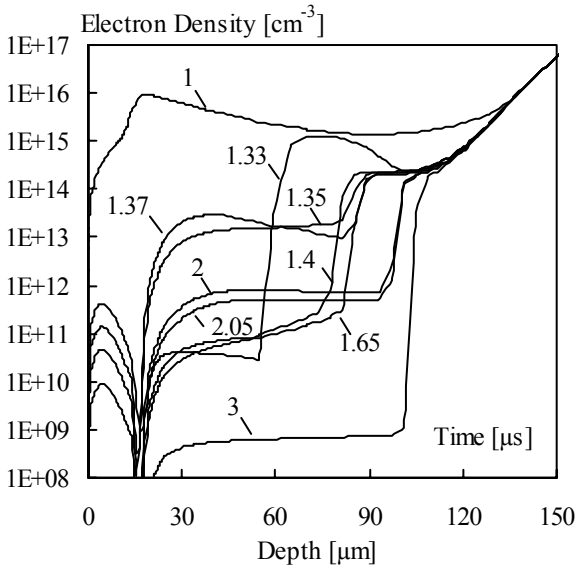

Fig. 5: Electron densities at different points in time, T=300K, V_R=800V, J_F=15A/cm^2

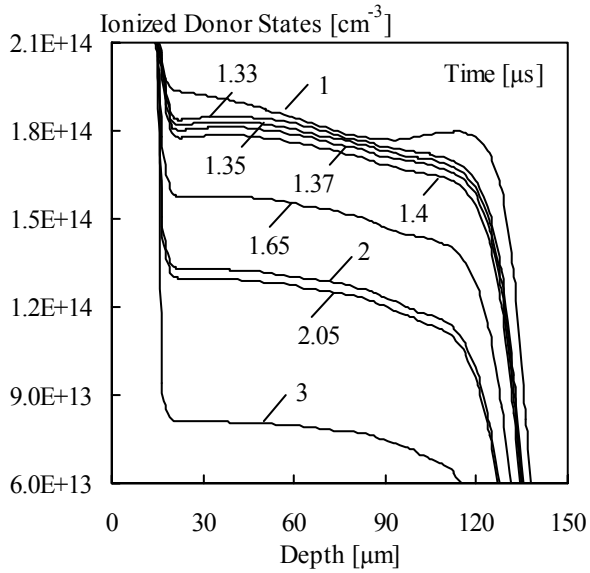

Fig. 6: Density of ionised donor-states vs. time, T=300K, V_R=800V, J_F=15A/cm^2

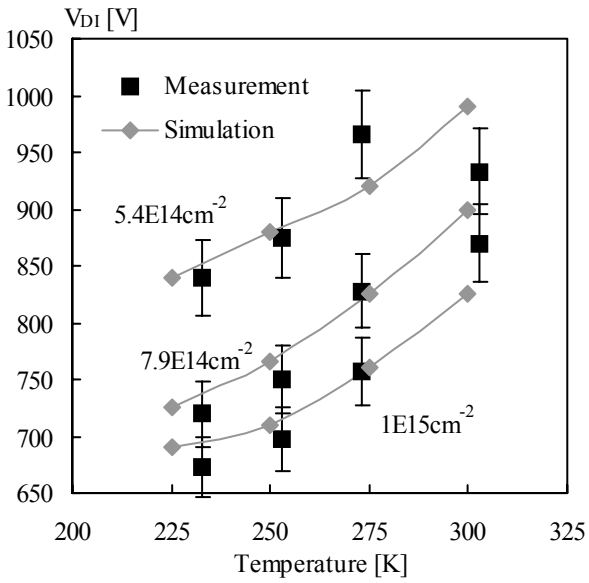

Fig. 7: Threshold voltage of impatt oscillation for 4.5MeV electron-radiated devices in dependence of temperature and irradiation dose. Measured values taken from [1]

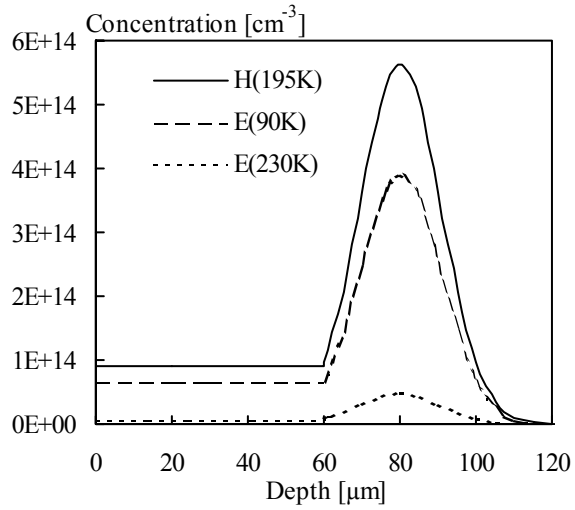

Fig. 8: Estimated recombination center profile of sample He21 for simulation

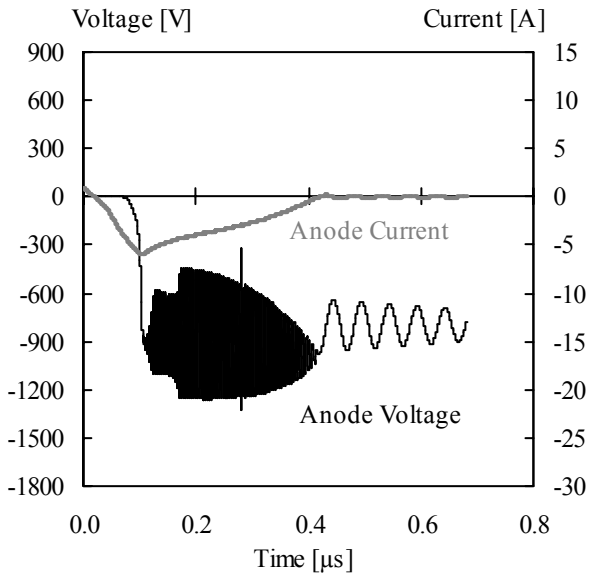

Fig. 9: Simulation of temporary impatt oscillation of a device with local recombination center distribution, T=300K, V_R=800V, J_F=15A/cm^2

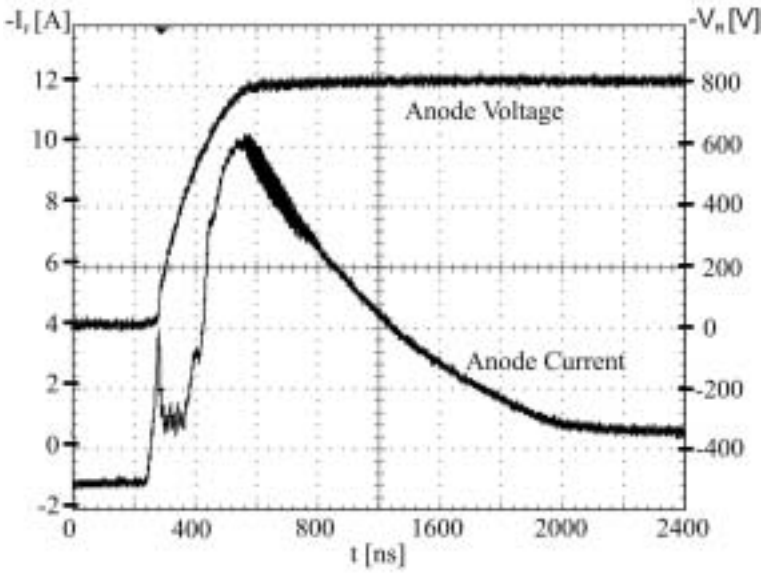

Fig. 10: Measurement of impatt oscillation at He21, T=275K, V_R=790V, J_F=15A/cm^2 (2A/div, 200V/div, 200ns)

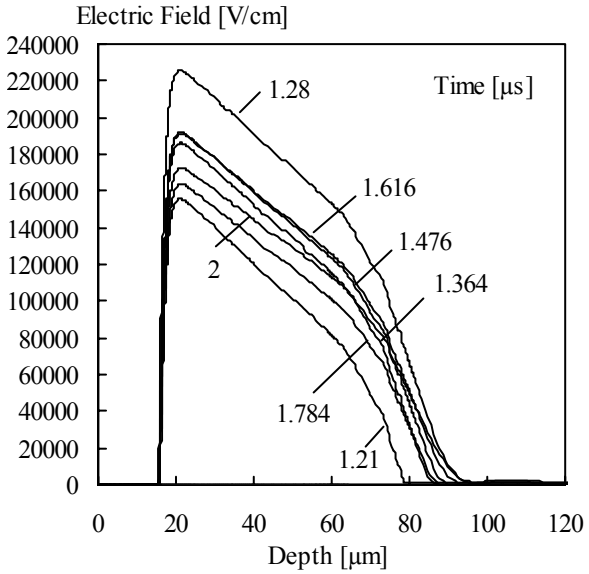

Fig. 11: Simulation of electric field along vertical axis vs. time for a helium-radiated diode structure, T=300K, V_R=800V, J_F=15A/cm^2

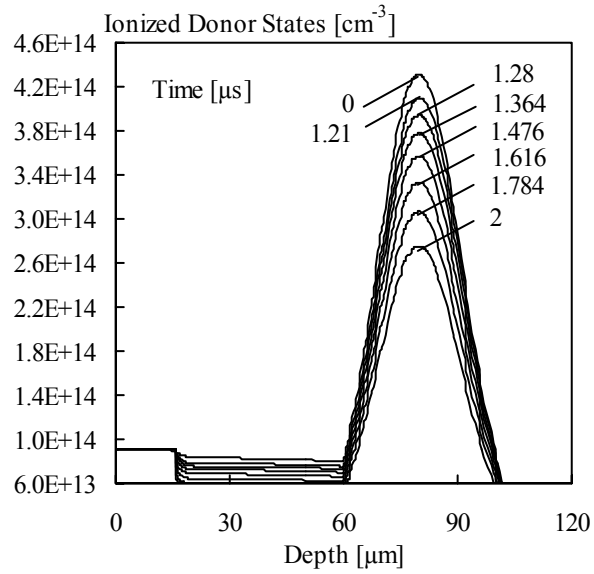

Fig. 12: Density of ionised donor-states vs. time in a simulated helium-radiated diode structure, T=300K, V_R=800V, J_F=15A/cm^2

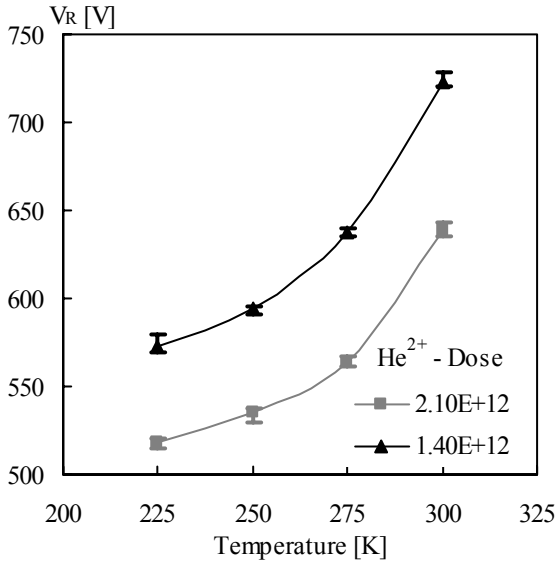

Fig. 13: Temperature dependence of reverse voltage for an avalanche current of 30A/cm^2 (helium-radiated samples)